An improved monomeric infrared fluorescent protein for neuronal and tumor brain imaging

Dan Yu[1,2], **William Clay Gustafson**[3], **Chun Han**[2,4,5], **Céline Lafaye**[8,9,10], **Marjolaine Noirclerc-Savoye**[8,9,10], **Woo-Ping Ge**[2,4,5], **Desiree A. Thayer**[2,4,5], **Hai Huang**[2,4], **Thomas B. Kornberg**[2,4], **Antoine Royant**[8,9,10,11], **Lily Yeh Jan**[2,4,5,6], **Yuh Nung Jan**[2,4,5,6], **William A. Weiss**[3,7], and **Xiaokun Shu**[1,2,*]

[1]Department of Pharmaceutical Chemistry, University of California, San Francisco, CA 94158

[2]Cardiovascular Research Institute, University of California, San Francisco, CA 94158

[3]Department of Pediatrics, Helen Diller Family Comprehensive Cancer Center, University of California, San Francisco, CA 94158

[4]Department of Biophysics and Biochemistry, University of California, San Francisco, CA 94158

[5]Department of Physiology, University of California, San Francisco, CA 94158

[6]Howard Hughes Medical Institute, University of California, San Francisco, CA 94158

[7]Departments of Neurology and Neurosurgery, Brain Tumor Research Center, University of California, San Francisco, CA 94158

[8]Université Grenoble Alpes, Institut de Biologie Structurale (IBS), F-38000 Grenoble, France

[9]CNRS, IBS, F-38000 Grenoble, France

[10]CEA, DSV, IBS, F-38000 Grenoble, France

[11]European Synchrotron Radiation Facility, F-38043 Grenoble, France

Abstract

Infrared fluorescent proteins (IFPs) are ideal for in vivo imaging and monomeric versions of these proteins can be advantageous as protein tags or for sensor development. In contrast to GFP, which requires only molecular oxygen for chromophore maturation, phytochrome-derived IFPs incorporate biliverdin (BV) as the chromophore. However, BV varies in concentration in different

cells and organisms. Here we engineered cells to express the heme oxygenase responsible for BV biosynthesys and a brighter monomeric IFP mutant (IFP2.0). Together, these tools improve the imaging capabilities of IFP2.0 compared to monomeric IFP1.4 and dimeric iRFP. By targeting IFP2.0 to the plasma membrane, we demonstrate robust labeling of neuronal processes in *Drosophila* larvae. We also show that this strategy improves the sensitivity when imaging brain tumors in whole mice. Our work shows promise in the application of IFPs for protein labeling and in vivo imaging.

The monomeric green and red fluorescent proteins (FPs) are powerful tools for multicolor protein labeling [1–3]. To add another labeling color and to open the application to whole-animal fluorescence imaging, we previously engineered a bacterial phytochrome into a monomeric IFP1.4 [4–6]. Because infrared light penetrates through tissue more efficiently than visible light [7,8], IFP1.4 outperforms far-red FP in imaging studies of liver in intact mice, even though the molecular brightness (quantum yield × extinction coefficient) of IFP1.4 is lower. Subsequently, another phytochrome-based IFP, iRFP, was developed and was shown to have molecular brightness that is similar to IFP1.4 but to have significantly higher brightness in cells (cellular brightness) [9]. And although the molecular brightness of other far-red fluorescent proteins with the GFP fold is higher, iRFP outperforms them in whole-animal imaging. iRFP is dimeric, however, which limits its application in protein labeling. We therefore decide to engineer a brighter monomeric IFP. Using directed evolution, we first improve the previously engineered monomeric IFP1.4 and name the new mutant IFP2.0, of which the cellular brightness is similar to iRFP. Because the chromophore of phytochrome-derived IFPs is converted from heme by the heme oxygenase 1 (HO1) and the activity of HO1 varies in different cells, we then engineer the cofactor biosynthetic pathway into cells and animals to further increase the brightness.

Our work demonstrates that the engineered cofactor biosynthesis significantly improves cellular brightness of IFP2.0 in human glial cells, primary neurons from mice, and peripheral neurons in intact *Drosophila.* The plasma membrane-targeted IFP2.0 (with HO1) successfully labels neuronal processes in *Drosophila*, whereas the plasma membrane-targeted iRFP fails with no detectable fluorescence in neuronal processes or soma. IFP2.0 and HO1 also improve tumor imaging in intact mouse brain, compared to iRFP. Our method will thus be useful in in vivo imaging.

Results

Directed evolution of IFP2.0

During directed evolution of the bacterial phytochrome DrBphP to IFP1.4 (Figure 1a), we observed that while disruption of the dimer interface in dimeric IFP1.2 led to monomeric IFP1.3, it significantly decreased the cellular brightness. Further engineering of IFP1.3 to IFP1.4 rescued the cellular brightness. Based on this, we reasoned that by combining the beneficial mutations of the dimeric IFP1.2 and the monomeric IFP1.4, we might be able to "breed" a brighter monomeric mutant. Through DNA shuffling followed by random mutagenesis [10,11], we developed the brighter, monomeric IFP2.0. IFP2.0 is slightly red shifted with excitation and emission maxima at 690 and 711 nm, respectively

(Supplementary Figure 1), compared to 684 and 708 nm for IFP1.4. Although IFP2.0 has similar quantum yield and extinction coefficient as IFP1.4 (Supplementary Table 1), it is significantly brighter (~13-fold, normalized to co-expressed GFP) when expressed in mammalian cells (HEK293) in the absence of exogenous BV (Supplementary Figure 2a). Sequence alignment of IFP2.0 with its ancestral forms: DrCBD (truncated form of DrBphP), IFP1.2 and 1.4, reveals several reverse mutations from IFP1.4 to 1.2, as well as several new mutations (Supplementary Figure 3). Since the cellular brightness is dependent on both molecular brightness and holoprotein concentration, our results suggest that the holo-IFP2.0 concentration is higher than holo-IFP1.4, due perhaps to increased protein solubility, stability, and BV binding affinity. iRFP has been shown to have similar characteristics [9].

Crystal structure of IFP2.0

While understanding the exact biophysical mechanisms will require further characterization, we solved the crystal structure of IFP2.0 at atomic resolution (1.14 Å), which so far is the highest resolution structure of proteins in the phytochrome family (Figure 1b, Supplementary Figure 4, Supplementary Table 2). The overall structure revealed that the protein scaffold was significantly evolved with root-mean-square deviation of atomic positions, 0.96 Å, between IFP2.0 and DrCBD (PDB entry code 2O9C) (Supplementary Figure 4b). These changes resulted in a more compact structure of IFP2.0, which may have improved protein folding, solubility, and stability. We located the eleven mutations in IFP2.0 relative to IFP1.4: one mutation (L6Q) is at the N-terminal loop; three mutations (E80D, A87T, P94Q) are in the PAS domain; and seven mutations (T168S, F198Y, H207T, M186V, E307Y, K311L, G314L) are in the GAF domain. Interestingly, four of the seven mutations in the GAF domain are reverse mutations from IFP1.4 to IFP1.2. Three mutations are near the chromophore (F198Y, H207T, M186V). H207 is the closest mutated residue to the chromophore, and the introduced His → Thr is a significant change. Therefore, H207T may be one of the key mutations responsible for the improved cellular brightness. Indeed, introduction of H207T into IFP1.4 improved the cellular brightness ~ 3-fold (Supplementary Figure 2b), supporting the idea that this residue is an important one and suggesting that further improvement may be possible via saturation mutagenesis of this residue or other residues near this position.

The crystal structure also provides potential mechanisms of engineered fluorescence of IFP1.4. Compared to the nonfluorescent DrCBD, one of the key mutations in IFP1.4 is A288V. V288 may function as a "clamp" that locks up the third ring of the chromophore through van der Waals interaction (Supplementary Figure 4d – f), and contributes to the fluorescence. Mutations at positions 195, 196 and 198 result in a cation-pi interaction between Arg172 and Tyr198, which rigidifies two β-strands in the vicinity of the 4th ring of the chromophore (Supplementary Figure 4b) and most likely favors radiative decay of the chromophore's excited state.

Stoichiometry of IFP2.0

Size exclusion chromatography indicates that IFP2.0 is monomeric (Supplementary Figure 5), although it retains only one (V318R) of the four mutations (Y307E, L311K, L314G, V318R) in IFP1.3 that are at the dimer interface of the wild type protein DrCBD

(Supplementary Figure 3). The crystal structure of IFP2.0 also revealed that the dimer interface present in DrCBD is no longer present in IFP2.0. These features suggest that V318R is sufficient to favor the monomeric form, a result that may be relevant to monomerizing other dimeric bacteriophytochrome-derived fluorescent proteins such as iRFP.

Engineering the cofactor biosynthesis pathway

As noted above, the phytochrome derived IFPs require the non-fluorescent BV as the cofactor (Figure 1c). BV is the initial catabolic product of heme by the heme oxygenase (HO1). Its endogenous concentration is thus expected to vary over wide ranges between different cell types, depending on the activity of HO1. We analyzed three different cell types in addition to the HEK293 line, and found that the infrared fluorescence of all the IFPs (including IFP1.4, IFP2.0, and iRFP), which was normalized by co-expressed GFP, was the lowest in primary hippocampal neurons (Figure 1d). The infrared fluorescence in HeLa cells was significantly higher than in hippocampal neurons and the fluorescence in the glial tumor cell line (glioblastoma) LN229 was intermediate (Figure 1d). Because of its potential importance to neurobiology and the advantage that might be conferred by adding another color to other FP-related methods such as the Brainbow technology that has been used to label different types of neurons [12], we decided to engineer the cofactor biosynthetic pathway for robust infrared fluorescence in neurons. We first co-expressed HO1 with IFP2.0 in neurons and observed that the fluorescence of IFP2.0 increased to a level similar to that in HeLa (Figure 1d, e). Co-expression of HO1 increased the cellular brightness of LN229 glial tumor cells by ~ 2-fold, but had no apparent effect in HeLa cells. These results suggest that engineering BV biosynthesis might overcome variations of endogenous BV concentration in different types of cells, and can increase the utility and applicability of IFP technology as a genetically encoded tag.

We studied potential effects of HO1 expression in the primary neurons. First, we observed that cultured neurons that over-express HO1 formed normal neuronal networks with no apparent differences compared to those without HO1 overexpression (Supplementary Figure 6). Second, we recorded electrophysiological properties of the neurons expressing IFPs and found no differences in the membrane potential or amplitude of action potentials among the control neurons (without expressing any exogenous gene) and four groups of neurons expressing IFP1.4; IFP2.0; iRFP; IFP2.0 with HO1 (Supplementary Figure 7). Therefore, we found no evidence that HO1 expression introduces morphological or functional changes to the primary neurons.

Expressing IFP2.0 in neurons of *Drosophila*

Based on these results, we then evaluated if IFP2.0 could be used to label neuronal processes in *Drosophila*. Previously it has been shown that by targeting GFP to the plasma membrane using the transmembrane domain of the human CD4 protein (CD4-GFP), significantly larger number of dendrites can be labeled than by GFP [13]. We therefore created three transgenic lines: CD4-IFP2.0 + HO1 (with the "self-cleaving" 2A peptide sequence [14] between IFP2.0 and HO1); CD4-IFP2.0; and CD4-iRFP. All the constructs were inserted into the same genomic locus and were driven by the same driver that labels dendritic arborization (da)

neurons [15]. CD4-IFP2.0 + HO1 robustly labeled da neurons, including the cell body, axon and dendrites (Figure 2a), with strong signal to background ratio (~10) (Figure 2b). Furthermore, smaller processes like dendritic spikes (terminal protrusions found in da neurons) were also visible (Figure 2d, e). Without HO1, however, the labeled da neurons had very dim cell body fluorescence (~10 times lower); and neuronal processes, including the dendrites, could not be clearly distinguished from the background (Figure 2c, f). Expression of CD4-iRFP did not generate any detectable fluorescence in da neurons, even after we increased the brightness 5-fold so that the unlabeled tracheal tube could be detected due to light scattering (Figure 2g). The tracheal tube is known to reflect light, which has been exploited in studying phenotypic change of tracheal system using reflected-light imaging [16]. These results demonstrate that first the IFP2.0 fusion is correctly targeted to the cell membrane and is a functional fusion tag. Secondly, the endogenous BV concentration is low in da neurons and therefore engineering of BV biosynthesis is necessary to image neuronal processes in *Drosophila*. Importantly, this engineered HO1 expression had no effect on development of the animal since the transgenic line develops normally with no observable phenotypic change.

Expressing IFP2.0 in other tissues of *Drosophila*

We also expressed the IFP constructs in the *Drosophila* trachea and wing imaginal discs and observed similar results. For these experiments, we co-expressed CD8-GFP in order to label cell membranes with both GFP and IFP. The transgenic lines expressing HO1 in trachea and wing disc both developed normally. CD4-IFP2.0 + HO1 labeled tracheal (Supplementary Figure 8) and wing disc (Supplementary Figure 9) cells strongly and the infrared fluorescence co-localized with GFP fluorescence. In contrast, the CD4-iRFP labeled cells were not fluorescent (Supplementary Figure 8 and 9), although iRFP (not fused to other proteins) was fluorescent in the tracheal tube and membrane-associated CD8-GFP fluorescence was robust (Supplementary Figure 8). These results demonstrate that the dimeric iRFP fails to label cell membranes in *Drosophila* using CD4-based approach, presumably because the dimerization by iRFP interferes with CD4 trafficking to the plasma membrane. Our results therefore suggest that in contrast to iRFP, CD4-IFP2.0 fusion will be a valuable reagent in protein labeling [17,18].

Expressing IFP2.0 in mouse brain tumors

In addition to providing an orthogonal color for protein labeling [19,20], another advantage of IFPs is its efficient light penetration for deep tissue imaging in whole-animals [21–23]. Previously, IFPs including IFP1.4 and iRFP have been used to image liver in intact mice. Encouraged by the robust expression in cultured neurons and glial cells, we investigated the use of IFP2.0 to image the tumors in the mouse brain. The principal challenges for this context are its requirement for the BV chromophore and the uncertain BV concentration in the brain, the presence of the skull, and the deep setting of many parts of the brain.

We used a glioma model for brain imaging. We first made two lentiviral constructs expressing IFP2.0 + HO1 and iRFP, respectively. Then we established stable cell lines of LN229, which is a glioma cell line established from cells taken from a patient with right frontal parieto-occipital glioblastoma [24]. Orthotopic tumors were grown by implanting the

cells into the right frontal lobe of a mouse brain (five mice per cell line). At the 4th week post implantation, we examined brains in whole animals for tumor fluorescence. Because the excitation and emission maxima of IFP2.0 and iRFP are similar (690/711 and 693/712 nm respectively), we used the same excitation (675 ± 15 nm) and emission (720 ± 10 nm) filters for imaging. The brain tumor expressing IFP2.0 + HO1 was strongly fluorescent in intact living mice (Figure 3a), suggesting that the infrared fluorescence penetrates through skull efficiently [25]. Importantly, the fluorescence signal was well-localized, indicating low scattering of the infrared fluorescence [26]. By comparison, the iRFP-expressing tumor was ~3-fold dimmer (Figure 3a, b). We also imaged brains that had been extracted from such animals and found that the images were consistent with the whole-animal fluorescence: that the IFP2.0 + HO1-marked tumors were significantly brighter (Figure 3c). Both IFP2.0 and iRFP tumors were in the right frontal lobe of the mouse brain. The brains were then sliced, which revealed similar tumor size. The brain slices were imaged by confocal microscopy, which revealed infrared fluorescent glioma cells (Figure 3d). The cells expressing IFP2.0 + HO1 in the brain slice were ~ 3 times brighter than the cells expressing iRFP (Figure 3d). Without HO1, however, IFP2.0-expressing tumor had similar brightness compared to iRFP (Supplementary Figure 10). The engineering of the co-factor biosynthesis pathway thus significantly improves brain imaging in mice. Based on these imaging results from intact mice, extracted brains and brain slices, we conclude that IFP2.0 + HO1 is significantly better (~3-fold) than iRFP for imaging these brain tumors in intact mice.

Discussion

We have engineered a bright monomeric IFP2.0. It is significantly brighter than IFP1.4 in cells, and is similar to the dimeric iRFP. We demonstrate that IFP2.0 tagged to CD4 labels the cell membrane in da neurons and other tissues of *Drosophila*, whereas CD4_iRFP fusion fails to label the cell membrane. Therefore, IFP2.0 is suitable for protein labeling at infrared wavelengths, which adds an orthogonal color to green and red fluorescent proteins. IFP2.0, therefore, provides a new opportunity and dimension in the study of protein-protein and cell-cell interactions.

In contrast to GFP that provides the chromophore by itself requiring only oxygen for the maturation, phytochrome-derived IFPs incorporate the endogenous molecule BV as the chromophore. We discover that in primary hippocampal neurons, the cofactor BV is limited. Engineered biosynthesis of BV significantly improved the brightness of IFP2.0 and therefore it enhances neuronal imaging using IFP2.0 as well as other IFPs. We find that BV is also limited in the da neurons in *Drosophila*, and that the engineered biosynthesis pathway enables us to image neuronal processes including dendrites and dendritic spikes in intact *Drosophila* larvae. Our method will therefore have useful applications in biological studies based on this important model organism. For example, because IFP2.0 is orthogonal to other visibly fluorescent proteins, plasma membrane-targeted IFP2.0 may be used to study how neuronal circuits are established through cell-cell interactions.

We also demonstrate that IFP2.0 and the engineered BV biosynthesis enable us to image brain tumor in intact mice, with significantly improved fluorescence intensity compared to iRFP. This imaging method will be useful in biomedical imaging study of glioblastoma. For

example, compared to luciferase, IFP2.0 not only allows whole-body imaging, but also cellular and subcellular imaging as well as cell sorting. Therefore, IFP2.0 together with HO1 may provide an opportunity to study early events during the development of glioblastoma and to sort and identify potential precursor cells. Our method may also be used to study tumor metastasis with better spatial resolution than luciferase and visibly fluorescent proteins, due to efficient penetration of infrared light through tissues.

Since there are many phytochrome sequences available [27,28], our structural and engineering work may serve to guide future engineering of brighter and monomeric phytochrome-derived IFPs, as well as IFPs with other photo-physical and -chemical properties.

Methods

Gene mutagenesis and screening

Genetic libraries were constructed by DNA shuffling using IFP1.4 and IFP1.1 as substrates followed by random mutagenesis. To prepare genes to be shuffled, about 10 ug plasmids containing IFP1.4 and IFP1.1 gene were digested at 37 °C for 1 h with BamH1 and EcoRI. Fragments of ~1kb were purified from 1% agarose gels using zymoclean gel DAN gel recovery kit (Zymo Research). The DNA concentrations were measured and the fragments were mixed 1:1 for a total of ~2ug. The mixture was digested with 0.5 unit DNase I (New England Biolabs) in 25 μl of 10mM Tris-HCl (pH7.6), 2.5mM $MgCl_2$ and 0.5mM $CaCl_2$ at 15°C for 13 min and terminated by heating at 95°C for 10 min. The DNase I digests were run on a 2% agarose gel and the size of 50–100 bp fragments were cut and purified by zymoclean gel DAN gel recovery kit (Zymo Research). 10 μl purified fragments were added to 10 μl Phusion® High-Fidelity PCR Master Mix and reassembled with a PCR program of 30 cycles, with each cycle consisting of 95°C for 60 s, 50°C for 60 s, and 72°C for 30 s. After gene reassembly, 1 μl of this reaction was amplified by PCR. Shuffled mutant library was expressed in in E. coli strain TOP10 and grown overnight on LB/agar (supplemented with 0.02% (wt/vol) L- arabinose (Sigma) at 37 °C and screened by imaging the agar plates with colonies using a BioSpectrum Imaging System (UVP, Upland, CA) in the APC channel (720nm) illuminated by 690nm light. The brightest clone of the shuffled library was used as template and subjected to four rounds of random mutagenesis. Random mutagenesis was performed with a GeneMorph II Random Mutagenesis Kit (Stratagene). Mutant libraries were expressed and screened as described above. The brightest clone in each library was picked as template for the next round of random mutagenesis.

Protein purification and characterization

IFP1.4, IFP2.0 and iRFP were expressed with C-terminal polyhistidine-tag on a pBAD expression vector (Invitrogen). Proteins were purified with the Ni-NTA purification system (Qiagen). Protein concentration was measured by the BCA method (Pierce). The extinction coefficients were based on a comparison of absorbance values for the protein at the main peak (692 nm or 694 nm) with the absorbance value at the 391 nm peak assuming the latter to have the extinction coefficient of the free BV, which is 39,900 M^{-1} cm^{-1}. For determination of quantum yield, fluorescence signal of IFP2.0 was compared to that of the

equally absorbing IFP1.4, iRFP and Alexa Fluor 647 dye (quantum yield is 0.33 in PBS, Invitrogen).

Protein expression and purification for crystallography

6xHis-tagged recombinant protein was expressed in Escherichia coli CodonPlus (DE3) RIL Cells (Stratagene). 1L LB broth medium containing 1 mM Ampicillin, was inoculated with 10 ml of an overnight culture at 37 °C. At an OD_{600} of approximately 0.6, expression of recombinant IFP2.0 was induced by the addition of 0.02% of arabinose and cells were grown for an additional 24 h at 37°C. Cells were pelleted by centrifugation (4000g, 4°C, 30 min), resuspended in buffer A (20 mM Tris-HCl pH 8.0, 500 mM NaCl), complemented with complete protease inhibitors-EDTA (Roche)) and disrupted using a sonicator. The soluble fraction was recovered by centrifugation (40 000g, 4°C, 30 min), and loaded on a 5 ml Ni-NTA superflow column (Qiagen) pre-equilibrated with buffer A. The His-tagged protein was eluted with 150 mM imidazole in buffer A. Fractions containing purified proteins were pooled and concentrated to 1 ml using Centricon devices (Amicon 30 000 Da cutoff) and loaded onto a size-exclusion chromatography column (Hiload Superdex 75, 10/300, GE Healthcare) for the final step of the purification procedure. The column was equilibrated with 20 mM Tris-HCl pH8.0 and the pooled peak fractions were concentrated to 18 mg/ml. The purity of the protein solutions was confirmed by SDS-PAGE. The final concentration was determined by UV spectroscopy assuming molar absorption coefficients at 280 nm of 34, 045 M^{-1} cm^{-1}.

Crystallization

Initial trials were performed using the sitting-drop method and commercial crystallization screening kits from Qiagen and Hampton Research. For the initial trials, we used a Cartesian PixSys 4200 crystallization robot (Genomic Solutions, U.K.) using 96-well Greiner Crystal Quick plates (flat bottom, untreated). 0.1 μl protein solution was mixed with 0.1 μl reservoir solution and the resulting drops were equilibrated against 100 μl reservoir solution. After optimization of the conditions, the best IFP2.0 crystals grew at room temperature in 28 % PEG 400, 0.1 *M* Sodium acetate pH 4.6. in 1–1.5 μl hanging drops using the vapor diffusion method.

X-ray diffraction data collection and structure refinement

Prior to diffraction experiments, crystals were flash-cooled directly in liquid nitrogen. X-ray diffraction experiments were performed at the European Synchrotron Radiation Facility (Grenoble, France). Data were collected at 100 K at a wavelength of 0.873 Å on beamline ID23-eh2. Diffraction data sets were processed using *XDS* [29] and intensities were scaled and reduced with *AIMLESS* [30]. The crystal belongs to the C2 space group and diffracted to 1.14 Å resolution. The solvent content is 46 %. Structure refinement was conducted with Refmac5 using anisotropic B-factors [31]. The thioether bond between Cys24 and the chromophore biliverdin appears to be X-ray sensitive. Structure and experimental data have been deposited in the Protein Data Bank under the PDB ID 4cqh. Crystallographic data statistics can be found in Table S2 of the Supplementary Information.

Gel filtration chromatography

Gel filtration chromatography was performed using a Superdex-200 HR 10/30 FPLC gel filtration column (Amersham Biosciences). The column was equilibrated with sterile phosphate buffered saline (PBS) in a cold room. 100 ul-purified proteins at a concentration of 0.5mg/ml in PBS were loaded on the column. Elution was performed in PBS, at a flow rate of 0.5ml/min for 45 min. The column effluent was monitored by absorbance at 280 and 630 nm. Gel filtration standard proteins of throglobulin, BSA, azurin and aprotinin were also loaded under the same conditions to calibrate the column. The linear calibration curve representing the logarithm of molecular mass as a function of the fraction number was used to calculate the molecular mass of the IFP2.0.

Characterization in mammalian cells and neurons

For characterization in mammalian cells, IFP1.4, IFP2.0, IFP2.0+HO1 and iRFP were cloned into pcDNA3.1 vector under CMV promoter. We also cloned GFP under internal ribosome entry site into the same vector. HEK293A cells were transfected using calcium phosphate transfection method and then imaged 48 h later on a Nikon eclipse Ti inverted epifluorescence microscope with redshifted Cy5.5 filter set (665/45 nm exciter and 725/50 nm emitter, Chroma) and a digital CMOS camera, controlled by NIS-Element software (Nikon Instruments). Images were processed and analyzed with ImageJ. The fluorescence intensity of IFPs was normalized by the fluorescence intensity of co-expressed GFP, to accommodate variations in transfection efficiency among cells.

For characterization in neurons, hippocampi were dissected from 19-d embryonic rats (E19), digested with a mixture of proteases at 37°C for 15 min and dissociated with a fire-polished Pasteur pipette in plating medium (minimal essential medium [MEM] containing Earle's salts with 10% fetal bovine serum, 0.5% glucose, 1 mM sodium pyruvate, 25 μM glutamine, and $1 \times$ penicillin/streptomycin). Neurons were then plated onto glass coverslips (Warner Instruments) pretreated with nitric acid and coated with poly-l-lysine (0.1 mL/mL; Sigma-Aldrich). Each 12-mm coverslip was plated with 5×10^4 neurons, which were maintained in neurobasal medium (Invitrogen) containing B27 extract (Invitrogen), 0.5 mM glutamine, 100 units of penicillin, and 100 μg/mL of streptomycin. Neuronal culture were incubated at 37°C with 5% CO2. For transient transfection, neurons in culture at 9 DIV were treated with Opti-MEM containing IFP1, 4, IFP2.0, IFP2.0+HO1 or iRFP plasmid, and Lipofectamine 2000 (Invitrogen). Images were taken 48h after transfection. Cells were imaged on a Zeiss Axiovert microscope with Cy5 filter set (Chroma) and a CoolSNAP ES2 CCD Camera (Photometrics, Tucson, AZ), controlled by MetaMorph software (version 7.6.2.0, Molecular Devices, Inc. Sunnyvale, CA). To perform whole-cell recording, recording pipettes were routinely filled with a solution containing (in mM): 125 K- gluconate, 15 KCl, 10 HEPES, 3 MgATP, 0.3 Na-GTP, 5 Na-phosphocreatine and 0.2 EGTA (pH 7.2–7.4, 290–300 mosM). The cells on coverslips were placed in an oxygenated (95% O_2 and 5% CO_2) solution containing 119 mM NaCl, 2.5 mM KCl, 2.5 mM $CaCl_2$, 1.3 mM $MgSO_4$, 1 mM NaH2PO4, 26.2 mM $NaHCO_3$, and 11 mM glucose. Action potentials were induced by injection of currents under current clamp.

Characterization in *Drosophila*

For characterization of neuronal processes in *Drosophila*, CD4-IFP2.0, CD4-IFP2.0+HO1 and iRFP were cloned into pACU2 vector (Addgene). Transgenic lines of CD4-IFP2.0 + HO1 (with the "self-cleaving" 2A peptide sequence 15 between IFP2.0 and HO1); CD4-IFP2.0; CD4-iRFP were created by ΦC31-mediated transformation at the *attP^{VK00019}* docker site. *Gal4$^{21-7}$* was used to drive the expression of the transgenes in all da neurons. For live imaging of larve, the animals were reared at 25°C in density-controlled vials. Third instar larvae at 96 hr after egg laying (AEL) were mounted in glycerol on glass slides. The dorsal da neuron cluster was imaged with a 40X NA1.25 oil lens on a Leica SP5 confocal microscope. For excitation of IFP2.0 and iRFP, 633 nm laser was used. Images shown are maximum intensity projections of image stacks covering da neuron layer (8–11 μm).

For characterization in the Drosophila tracheal tube, Btl-Gal4:UAS-CD8GFP flies were crossed with UAS-CD4-IFP2.0 or UAS-IFP2.0 transgenic flies. The IFP2.0, IFP2.0+HO1 and iRFP plasmids are inserted into the same locus at 3rd chromosome. For confocal imaging, flies were maintained on a cornmeal and agar medium at 25°C according to standard protocol. Wandering third instar larvae were collected and dissected in cold phosphate-buffered saline (PBS). Wing imaginal discs were placed in a droplet of 1XPBS buffer on the coverslip. The discs were gently flattened and attached to coverslips by reducing the amount of PBS. Then the coverslips were inverted on depression slides. The wing discs were hanging in the center of depression. Images were taken on a Nikon spinning disk confocal.

Construction of lentiviral vectors and cell transfection

To create Lentivirus expressing IFP1.4, IFP2.0, IFP2.0+HO1 or iRFP and GFP, a transcription unit comprising the IFP1.4, IFP2.0, IFP2.0+HO1 or iRFP coding sequence, the poliovirus IRES, and GFP was constructed by assembly PCR, cloned into pENTR1a (Invitrogen), and transferred into pLenti-CMV-DEST (Invitrogen) by Gateway recombinase (Invitrogen). Viruses were produced in HEK293 cells with ViraPower™ Lentiviral Expression System (Invitrogen) according to the manufacturer's recommendations and purified by anion exchange chromatography (FastTrap purification kit, Millipore), resuspended in HBSS + 10% glycerol, and stored in aliquots at −80°C. Titers as assessed on HEK293 cells by GFP fluorescence were 44000 infectious units (IU) per mL for each virus. For transfection, LN229 Cells were plated on 100 mm culture dishes and cultured to ~80% confluence. 3mL of virus aliquots and 3mL of fresh medium were mixed and added on the cells. Long-term transgene expression was maintained by selecting for resistance to puromycin at a final concentration of 10 μg/mL.

Intracranial Xenografts and *In vivo* mouse brain imaging

LN229 cells stably expressing IFP2.0, IFP2.0+HO1 or iRFP were cultured in H21 medium containing 10% FBS, harvested in logarithmic growth, and suspended at a density of 2×10^8 cells/mL in PBS at room temperature. For intracranial injection, 4- to 6-wk-old female BALB/c nu/nu mice (Harlan; Sprague–Dawley) were anesthetized (5 mice for each constructs) and a small surgical incision was made in the skin covering the skull 2 mm to the right of the bregma. Cell suspensions (5 μL) containing approximately 1×10^6 LN229 cells

at room temperature were slowly (~6 seconds) injected intracranially at 3.5 mm below the skull surface using a 29-gauge needle. Immediately thereafter the incision was closed with surgical adhesive and the animals were monitored until conscious and returned to their cages. Intracranial xenograft growth was assessed twice weekly. Tumors were established about 2 weeks after injections. All mouse experimentation was performed in accordance with protocols approved by the IACUC at the University of California, San Francisco and adhered to the National Institutes of Health Guide for the Care and Use of Laboratory Animals. Mouse imaging was performed with an IVIS Spectrum instrument (Caliper LifeSciences) in epifluorescence mode equipped with 675/30 nm and 720/20 nm filters for excitation and emission, respectively. All quantitative measurements of fluorescence signal were performed using the Living Image Software 4.0.

Confocal imaging of acutely isolated brain slices

Slices were prepared according to standard procedures. Mice were anesthetized with isoflurane and decapitalized. Mouse brains were dissected rapidly and sliced (400μM in thickness) with a vibratome (VT-1000S; Leica) in ice-cold oxygenated (95% O_2 and 5% CO_2) artificial cerebrospinal fluid solution (aCSF) containing 119 mM NaCl, 2.5 KCl, 2.5 mM $CaCl_2$, 1.3 mM $MgSO_4$, 1 mM NaH2PO4, 26.2 $NaHCO_3$ and 11mM glucose. The slices were imaged on a Zeiss LSM510 confocal microscope equipped with objective 63×/ 0.9W (Zeiss). Slices were scanned by 633nm laser in xyz mode with 8 μm interval between slices. Projection images were made from z-stacks. During imaging, slices were kept in a chamber with perfusion of CSF at room temperature.

Supplementary Material

Refer to Web version on PubMed Central for supplementary material.

Acknowledgments

References

1. Kremers GJ, Gilbert SG, Cranfill PJ, Davidson MW, Piston DW. Fluorescent proteins at a glance. Journal of Cell Science. 2011; 124:2676–2676.

2. Chudakov DM, Matz MV, Lukyanov S, Lukyanov KA. Fluorescent Proteins and Their Applications in Imaging Living Cells and Tissues. Physiological Reviews. 2010; 90:1103–1163. [PubMed: 20664080]

3. Tsien RY. Constructing and exploiting the fluorescent protein paintbox (Nobel Lecture). Angew Chem Int Ed Engl. 2009; 48:5612–5626. [PubMed: 19565590]

4. Wagner JR, et al. Mutational analysis of Deinococcus radiodurans bacteriophytochrome reveals key amino acids necessary for the photochromicity and proton exchange cycle of phytochromes. J Biol Chem. 2008; 283:12212–12226. [PubMed: 18192276]

5. Wagner JR, Brunzelle JS, Forest KT, Vierstra RD. A light-sensing knot revealed by the structure of the chromophore-binding domain of phytochrome. Nature. 2005; 438:325–331. [PubMed: 16292304]

6. Shu X, et al. Mammalian expression of infrared fluorescent proteins engineered from a bacterial phytochrome. Science. 2009; 324:804–807. [PubMed: 19423828]

7. Lecoq J, Schnitzer MJ. An infrared fluorescent protein for deeper imaging. Nat Biotechnol. 2011; 29:715–716. [PubMed: 21822247]

8. Rice BW, Contag CH. The importance of being red. Nat Biotechnol. 2009; 27:624–625. [PubMed: 19587667]

9. Filonov GS, et al. Bright and stable near-infrared fluorescent protein for in vivo imaging. Nat Biotechnol. 2011; 29:757–761. [PubMed: 21765402]

10. Stemmer WP. DNA shuffling by random fragmentation and reassembly: in vitro recombination for molecular evolution. Proc Natl Acad Sci USA. 1994; 91:10747–10751. [PubMed: 7938023]

11. Stemmer WP. Rapid evolution of a protein in vitro by DNA shuffling. Nature. 1994; 370:389–391. [PubMed: 8047147]

12. Livet J, et al. Transgenic strategies for combinatorial expression of fluorescent proteins in the nervous system. Nature. 2007; 450:56–62. [PubMed: 17972876]

13. Han C, Jan LY, Jan YN. Enhancer-driven membrane markers for analysis of nonautonomous mechanisms reveal neuron-glia interactions in Drosophila. Proceedings of the National Academy of Sciences. 2011; 108:9673–9678.

14. Szymczak AL, et al. Correction of multi-gene deficiency in vivo using a single 'self-cleaving' 2A peptide-based retroviral vector. Nat Biotechnol. 2004; 22:589–594. [PubMed: 15064769]

15. Jan YN, Jan LY. Branching out: mechanisms of dendritic arborization. Nature Publishing Group. 2010; 11:316–328.

16. Glasheen BM, Kabra AT, Page-McCaw A. Distinct functions for the catalytic and hemopexin domains of a Drosophila matrix metalloproteinase. Proceedings of the National Academy of Sciences. 2009; 106:2659–2664.

17. Roy S, Hsiung F, Kornberg TB. Specificity of Drosophila Cytonemes for Distinct Signaling Pathways. Science. 2011; 332:354–358. [PubMed: 21493861]

18. Affolter M, Basler K. Cytonemes Show Their Colors. Science. 2011; 332:312–313. [PubMed: 21493848]

19. Shaner NC, Steinbach PA, Tsien RY. A guide to choosing fluorescent proteins. Nat Methods. 2005; 2:905–909. [PubMed: 16299475]

20. Shaner NC, et al. Improved monomeric red, orange and yellow fluorescent proteins derived from Discosoma sp. red fluorescent protein. Nat Biotechnol. 2004; 22:1567–1572. [PubMed: 15558047]

21. Weissleder R, Ntziachristos V. Shedding light onto live molecular targets. Nat Med. 2003; 9:123–128. [PubMed: 12514725]

22. Schroeder T. Imaging stem-cell-driven regeneration in mammals. Nature. 2008; 453:345–351. [PubMed: 18480816]

23. Weissleder R, Pittet MJ. Imaging in the era of molecular oncology. Nature. 2008; 452:580–589. [PubMed: 18385732]

24. Ishii N, et al. Frequent Co-Alterations of TP53, p16/CDKN2A, p14ARF, PTEN Tumor Suppressor Genes in Human Glioma Cell Lines. Brain pathology. 1999; 9:469–479. [PubMed: 10416987]

25. Jöbsis FF. Noninvasive, infrared monitoring of cerebral and myocardial oxygen sufficiency and circulatory parameters. Science. 1977; 198:1264–1267. [PubMed: 929199]

26. Wilson BC, Jacques SL. Optical reflectance and transmittance of tissues: principles and applications. Quantum Electronics, IEEE Journal of. 1990; 26:2186–2199.

27. Giraud E, Verméglio A. Bacteriophytochromes in anoxygenic photosynthetic bacteria. Photosyn Res. 2008; 97:141–153. [PubMed: 18612842]

28. Karniol B, Wagner JR, Walker JM, Vierstra RD. Phylogenetic analysis of the phytochrome superfamily reveals distinct microbial subfamilies of photoreceptors. Biochem J. 2005; 392:103. [PubMed: 16004604]

29. Kabsch W. research papers. Acta Cryst. 2010; D66:125–132.10.1107/S09074449090473372010:1–8.10.1107/S0907444909047337

30. Evans PR. research papers. Acta Cryst. 2011; D67:282–292.10.1107/S090744491003982X2011:1–11.10.1107/S090744491003982X

31. Murshudov GN, et al. REFMAC5 for the refinement of macromolecular crystal structures. Acta Cryst. 2011; D67:355–367.10.1107/S09074449110013142011:1–13.10.1107/S0907444911001314

32. Thayer DA, Jan YN, Jan LY. Increased neuronal activity fragments the Golgi complex. Proc Natl Acad Sci USA. 2013; 110:1482–1487. [PubMed: 23297202]

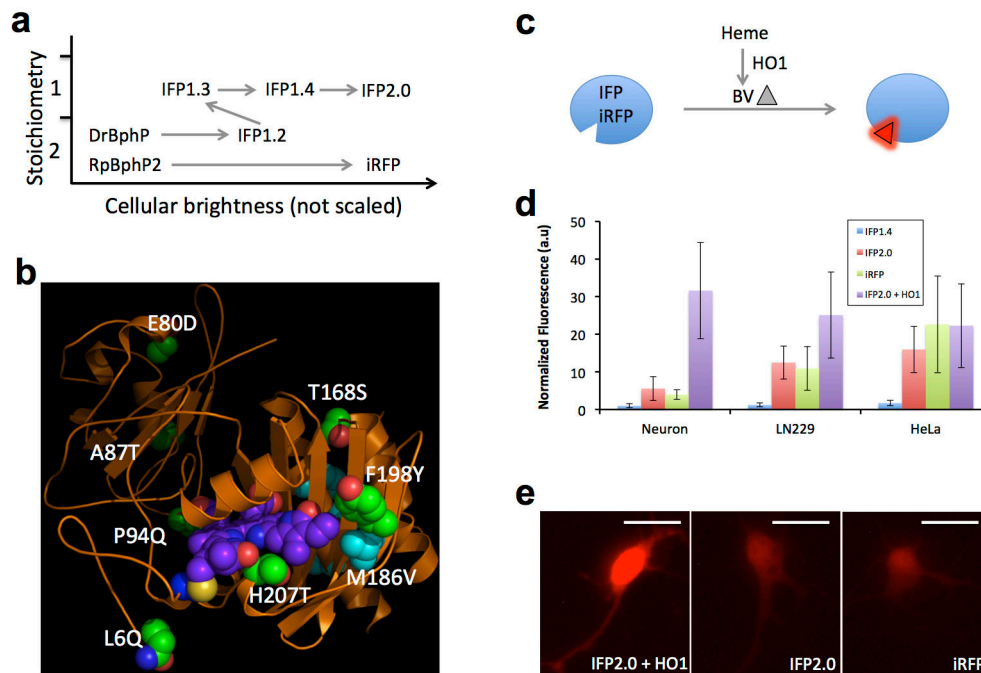33. Ge WP, Miyawaki A, Gage FH, Jan YN, Jan LY. nature10959. Nature. 2012; 484:376–380. [PubMed: 22456708]

Figure 1.

Directed evolution of a bright and monomeric infrared fluorescent protein (IFP2.0) and engineering of its cofactor biosynthesis. (**a**) Schematic diagram showing directed evolution of IFP2.0. (**b**) Crystal structure of IFP2.0 at atomic-resolution (1.13 Å). The mutations relative to IFP1.4 are labeled. 7 (in green) of 11 mutations are newly introduced, the remaining 4 (in cyan) are reverse mutations from IFP1.4 to IFP1.2. 3 of these 4 are located at the c-terminus (barely seen behind the chromophore, Fig. S3). BV is shown in purple. (**c**) Phytochrome-based IFPs and iRFP incorporate BV as the chromophore, which is an initial product of heme by heme oxygenase (HO1) and becomes fluorescent only when bound to IFPs. (**d**) Comparison of the cellular brightness of IFP1.4, IFP2.0, iRFP, and IFP2.0 + HO1 in three cell types: primary hippocampal neuron, glioma cell LN229 and cervical cancer cell HeLa. Fluorescence is normalized by co-expressed GFP. The error bar represents standard deviation (n = 10). (**e**) Representative fluorescence images of neurons showing significant increase of cellular brightness by co-expression of HO1. Scale bar, 40 μm.
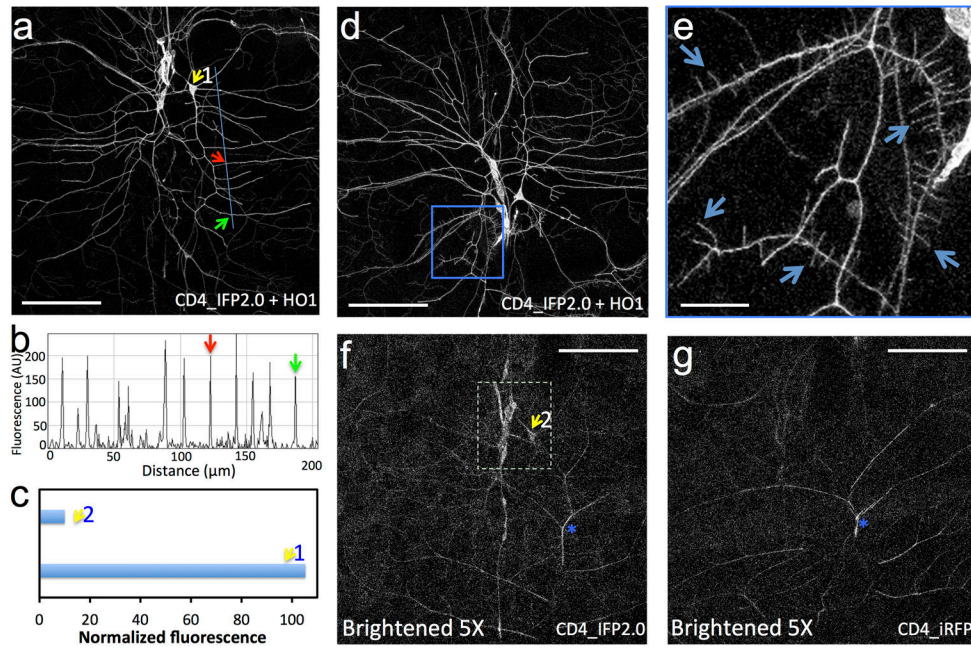
Figure 2.
IFP2.0 with engineered biosynthesis of the cofactor improves neuronal imaging in *Drosophila* larvae Cellular membrane of dendritic arborization (da) neurons labeled by (**a, d, e**) IFP2.0 fused to CD4 with expression of HO1 that produces the cofactor (CD4-IFP2.0 + HO1); (**f**) CD4-IFP2.0; (**g**) CD4-iRFP. (**b**) Fluorescence intensity profile along the line in (**a**); the green and red arrow point to the dendrites in (**a**). (**c**) Normalized fluorescence intensity of the cell body pointed by the yellow arrow in (**a**) and (**f**). (**e**) Confocal image of the area (blue box) in (**d**), with arrows pointing to dendritic spikes. Scale bar: (a, d, f, g), 100 μm; (e), 20 μm.
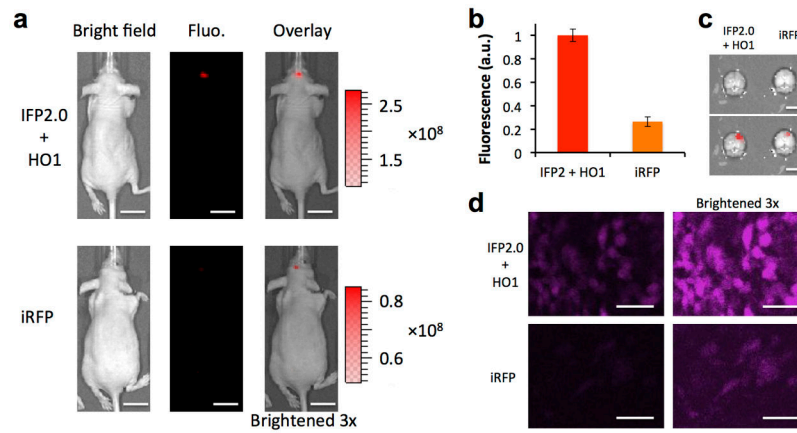
Figure 3.
IFP2.0 with engineered biosynthesis of the cofactor improve imaging of tumors in mice. (**a**) Bright field (left), fluorescence (middle), and overlay (right) images of the brain tumor (glioblastoma) in intact mice expressing IFP2.0 + HO1 (top), iRFP (bottom). The fluorescence intensity in the overlay image of iRFP is 3-fold (3x) brightened compared to that of IFP2.0 + HO1. The scale bar indicates fluorescence radiant efficiency. (**b**) Average fluorescence intensity of the brain tumor in intact mice with standard deviation. (**c**) Bright field (top) and fluorescence overlay (bottom) images of the extracted brain. (**d**) Confocal images of the brain slices. The right panels show 3x brightened images. Size scale bar: (a), 1 cm; (c), 3 mm; (d), 40 μm.